*Journal of Computer-Aided Molecular Design* **19:** 1–15, 2005.
DOI 10.1007/s10822-005-0096-7



# Protonation-induced stereoisomerism in nicotine: Conformational studies using classical (AMBER) and *ab initio* (Car–Parrinello) molecular dynamics

Philip S. Hammond*[,1], Yudong Wu[2,3], Rebecca Harris[1], Todd J. Minehardt[4], Roberto Car[2] & Jeffrey D. Schmitt[1]

[1]*Targacept, Inc., 200 East First Street, Suite 300, Winston-Salem, NC 27101-4165, USA;* [2]*Department of Chemistry, Princeton University, Princeton, NJ 08544, USA;* [3]*Present address: Department of Chemistry and Chemical Biology, Harvard University, 12 Oxford Street, Cambridge, MA 02138, USA;* [4]*N Space Labs, Inc., 39 W. 14th St., Suite 404, New York, NY 10011, USA*

Received 25 August 2004; accepted in revised form 29 December 2004


*Key words: ab initio* molecular dynamics, AMBER, Car–Parrinello, nicotine, nicotinic acetylcholine receptors, protonation-induced stereoisomerism

**Summary**

A variety of biologically active small molecules contain prochiral tertiary amines, which become chiral centers upon protonation. S-nicotine, the prototypical nicotinic acetylcholine receptor agonist, produces two diastereomers on protonation. Results, using both classical (AMBER) and *ab initio* (Car–Parrinello) molecular dynamical studies, illustrate the significant differences in conformational space explored by each diastereomer. As is expected, this phenomenon has an appreciable effect on nicotine's energy hypersurface and leads to differentiation in molecular shape and divergent sampling. Thus, protonation induced isomerism can produce dynamic effects that may influence the behavior of a molecule in its interaction with a target protein. We also examine differences in the conformational dynamics for each diastereomer as quantified by both molecular dynamics methods.

*Abbreviations:* aiMD – *ab initio* molecular dynamics; ACh – acetylcholine; AChBP – acetylcholine binding protein; DFT – density functional theory; LGIC – ligand-gated ion channels; MM – molecular mechanics; nAChR – nicotinic acetylcholine receptors; QM – quantum mechanics; QSAR – quantitative structure activity relationships; SE – semi-empirical.

## Introduction

Nicotinic acetylcholine receptors (nAChRs) are ligand-gated ion channels (LGIC) that influence a variety of biological functions and are believed to play roles in various neurological and mental disorders. Compounds that modulate these receptors (nicotinic agonists and antagonists) are under investigation as potential therapeutics for pain, cognitive deficits, Alzheimer's and Parkinson's diseases, schizophrenia, ulcerative colitis, anxiety, depression, Tourette's syndrome among others [1].

Ligands known to modulate a variety of neuroreceptors of importance often contain pro-cationic centers of the type illustrated by nicotine. As is the case for many other drug-like compounds containing an asymmetrical tertiary

*To whom correspondence should be addressed. Fax: +1-336-480-2107; E-mail: phil.hammond@targacept.com

amine, protonation of nicotine results in chiral induction. For nicotine, this protonation-induced stereoisomerism leads to two different diastereomers, each presumably having different receptor or host binding properties. The S,S-diastereomer (**1a)** results from *re*-face attack and shows a *cis* arrangement of the bulky methyl and pyridyl substituents on the pyrrolidine ring (Figure 2). Alternatively, *si*-face attack results in the R,S-diastereomer (**1b)**, with the methyl group *trans* to the pyridine ring (Figure 2).

Whether one or both of these diastereomers contribute to the binding affinity of nicotine to nAChRs is unknown. Crystal structures of both protonated [2] and diprotonated [3] nicotine show the *trans* form for the monoprotonated species exists in the solid phase. It was concluded from early NMR studies of protonated nicotine that the *cis* form predominates [4], while later studies at low pH on the diprotonated form found a 10:1 *trans*/*cis* ratio in solution [5]. Elmore and Dougherty have recently examined the relative energies of low energy conformations of nicotine, protonated nicotine, and diprotonated nicotine both in the gas phase and in water, using several computational methods [6]. The conformational minima were identified using AM1 and MMFF94. Additional energetic comparisons using several levels of theory predict similar energies for the two *trans* conformers and a 3–4 kcal $mol^{-1}\Delta G$ difference between those and the higher energy *cis* conformers.

In typical three-dimensional quantitative structure activity relationship (3D QSAR) studies, the global minimum energy conformation or several low-energy conformations are selected from the potential energy hypersurface. These are used as starting points for further refinement prior to construction of SAR models (for an example based on nAChR ligands, see Gohlke et al. [7]). Recent reviews have discussed the role of protein flexibility and implications for the design of active ligands [8]. Compounds interacting with a receptor may take on a variety of conformations [9], either by binding to a number of pre-existing and energetically similar protein conformations or *via* induced fit. Therefore, it is likely that an ensemble of conformations may contribute to interactions with their biological targets, not just a single low energy conformation, and ensemble characteristics may be an important measure of a compound's conformational behavior.

Evidence suggests that $\pi$-cation interactions play a major role during binding of endogenous neurotransmitters as well as binding of small drug-like ligands with their target receptors (for a recent review see Zacharias and Dougherty [10]). Typically, these interactions arise from associations between the aromatic amino acid side chains of tryptophan, tyrosine or phenylalanine, and the cationic region of the ligand via an induced quadrapole interaction. $\pi$-Cation interactions may contribute as much as 3.6 kcal $mol^{-1}$ to the overall binding energy in water of methylammonium and benzene [11], while semi-empirical calculations estimate an upper limit for gas-phase interactions of 13 kcal $mol^{-1}$ [12]. A number of recent reviews have examined the nature of $\pi$-cation interactions [13, 14], with these interactions playing a key role in the recognition and binding of LGIC receptors, G-protein-coupled receptors, various neurotransmitter transporters and enzymes [15]. Thus, detailed conformational dynamics studies that accurately account for both ensemble characteristics and electronic charge distribution could aid in determining important features of molecular recognition, since interaction energies between diastereomers and receptor will likely be different.

Based on our interest in the development of nAChR therapeutics, we have undertaken a careful examination of the conformational behavior of protonated S-nicotine, the prototypical nicotinic agonist. Conformational ensemble population behavior for diastereomers **1a** (*cis*) and **1b** (*trans*) S-nicotine, produced by protonation of S-nicotine, have been examined by molecular mechanics using AMBER [16–18] and the *ab initio* molecular dynamics (aiMD) method [19–26]. In aiMD, throughout the trajectory the ground state of the system with an instantaneous set of nuclear coordinates is efficiently solved at the level of density functional theory (DFT). Valence electrons are included explicitly and allowed to move dynamically to account for important effects on the electronic state of a system.

Analysis of the data collected using these two methods show that dramatic differences exist between the (*cis*) and (*trans*) S-nicotine diastereomers. Further, while both methods give qualitatively similar results, differences do exist that may be a result of explicit evaluations of charge distribution effects during the course of the aiMD calculations.

## Computational details

Starting conformations for aiMD were obtained using Sybyl [27] Version 6.9 running on a Silicon Graphics Origin 3000 server, using the internal coordinate Monte Carlo search method [28–31] (Random Search, original option), and minimized using the Tripos Force Field. Settings used for random search were RMS Threshold = 0.200 Å, maximum cycles = 4000, maximum data hits = 6, data convergence = 0.005 kcal $\cdot$ mol$^{-1}$, maximum iterations = 4000, energy cutoff set to 10.0 kcal mol$^{-1}$ above the starting conformation, and default for the remaining minimizer settings.

The AMBER 7.0 software package [16, 18, 32] and the force field of Cornell et al. [33] were used for the classical MD simulations. Restrained electrostatic potential (RESP) charges [34] were obtained by fitting Gaussian 98 [35] charges in a manner similar to that described previously [36]. Other missing force field parameters were generated with AMBER's Antechamber [37] module. A 1 fs time step was used with periodic boundary conditions, and the weak-bath thermostat of Berendsen and coworkers [38] was employed. All structures were minimized *in vacuo* for 500 steepest descent steps followed by 500 steps of conjugate gradient minimization. Resulting structures were then used as initial points for MD simulations. The system was allowed to evolve for 2 ns at 800 K in the NVT ensemble.

Static quantum chemical calculations were performed using the orbital DFT implementation of Gaussian 98 (6-31G** orbital basis set) to characterize various points on the potential energy surfaces. These calculations were performed with a Becke three-parameter exchange and Lee–Yang–Parr correlation functional [39] (B3LYP) or the Perdew–Wang 91 (PW91) [40, 41] exchange–correlation functional. In contrast to the aiMD calculations, all electrons, including both core and valence are explicitly treated in Gaussian98.

The DFT-based Car-Parrinello package was used to perform aiMD simulations [42, 43] (plane-wave basis set and ultrasoft pseudopotentials for valence electrons). In aiMD, the Perdew-Burke-Ernzerhof (PBE) [44] generalized gradient approximation (GGA) was adopted for the exchange and correlation energy. Wavefunctions and charge density are accurately represented with energy cutoffs of $7.85 \times 10^3$ kcal mol$^{-1}$ (25 Ry) and $6.28 \times 10^4$ kcal $\cdot$ mol$^{-1}$ (200 Ry), respectively, using ultrasoft pseudopotentials. Molecules were placed in a cubic cell with a length of 13.23 Å. The cell was chosen so that interactions between atoms and their images in neighboring cells were negligible. In addition, since the systems under study were charged, cells were large enough that charge–charge interactions between neighboring cells did not affect conformational dynamics. To assure that this was the case, the Makov–Payne correction, which significantly improves the convergence properties of charged systems, was used to test our choice of cell size. Four distinct conformers (two for each diastereomer) were tested and showed an error smaller than 0.3 kcal mol$^{-1}$ in the energy difference between two molecules with the same diastereomer. Therefore, under these conditions our choice of size for the simulation cell was suitable for the systems studied.

Constant temperature aiMD was initiated by random displacement (10% of bond lengths) of atoms from their starting coordinates. Electron wavefunctions were converged to ground state, then both ions (nuclei with core electrons) and valence electrons were allowed to move freely. After 500 steps of free aiMD, the system was gradually heated with coupling to a Nose-Hoover thermostat [45]. The time step and fictitious electronic mass for aiMD were chosen to be 0.24 fs and 0.4 amu, respectively. After equilibration for 2000 steps, the system was maintained at 800 K with coupling to the thermostat (44 amu) during the sampling period. Use of the Nose-Hoover thermostat leads to sampling in the canonical ensemble. In a typical simulation, the temperature of the system exhibited a mean value of 799.8 K. For the same trajectory, the potential and kinetic energies of the system showed a standard deviation of 12.9 kcal $\cdot$ mol$^{-1}$and 0.2 kcal mol$^{-1}$, respectively.

To provide estimates of energy barriers for rotation around the inter-ring torsional bond (T1, Figure 1), geometry scans were carried out using the Jaguar suite of software from Schrödinger [46] at the DFT level with BLYP and 6-31G* basis set.

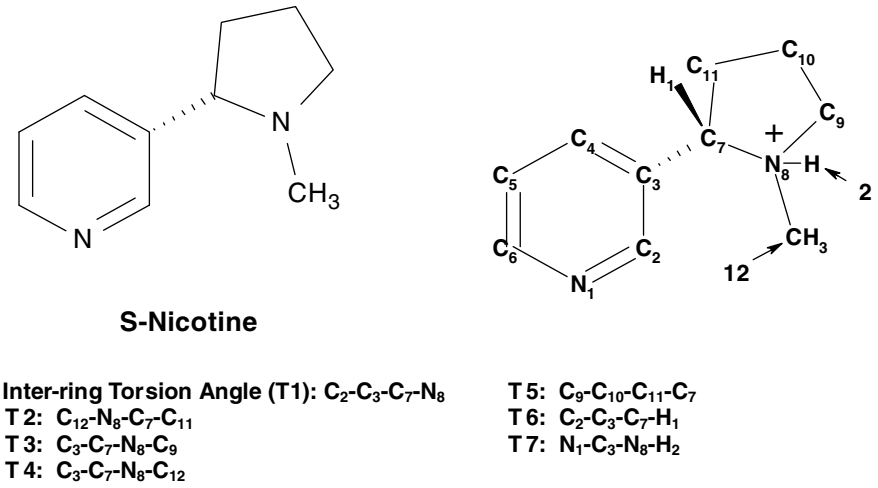


*Figure 1.* Structure of S-(−)-nicotine, numbering scheme used for protonated nicotine, and torsional angle definitions.

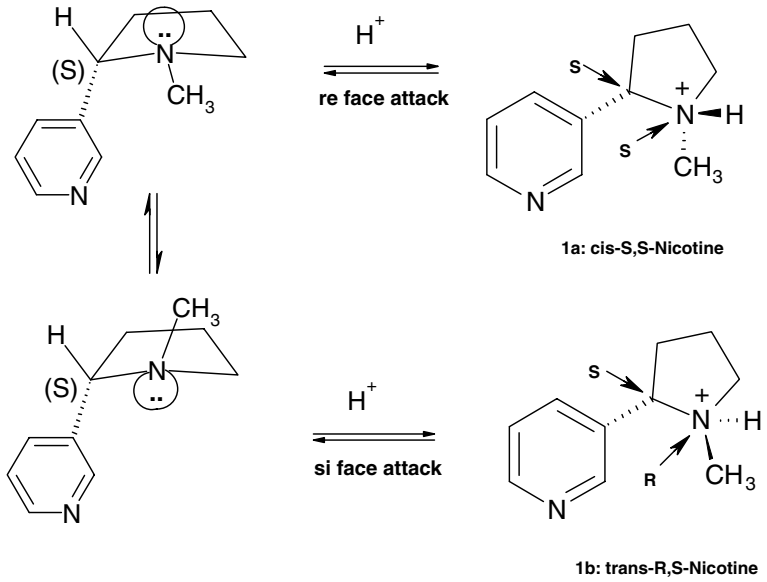


*Figure 2.* Protonation of S-(−)-nicotine leads to a pair of diastereomers that are expected to have differing binding affinities at nAChRs.

## Results and discussion

### *Static calculations*

Initially, low-energy conformations for both diastereomers of protonated S-nicotine were identified using the Tripos molecular mechanics (MM) force field. These were subsequently used as starting points both for single point calculations for a comparison of three different DFT methods, and, as starting points for ensemble dynamical simulations with aiMD. Fourteen local minima for **1a** (*cis* S,S-nicotine; Figure 2) and 10 local minima for **1b** (*trans* R,S-nicotine; Figure 2) were identified. Conformational details and energies for these sets of local minima are shown in Tables 1 and 2 [47]. Pairs of conformations (A1–B1, A2–B2, etc) for both diastereomers are similar, but with the cationic center located on opposite sides of the pyridine ring. The pyrrolidine ring of the lowest energy conformations for both diastereomers adopts an envelope conformation, with $C_9$ out-of-

*Table 1.* Geometry details for 14 local minima and approximate transition conformations of protonated *cis* nicotine.

| | Tors 1 $C_2$-$C_3$- $C_7$-$N_8$ | Tors 2 $C_{12}$-$N_8$-$C_7$-$C_{11}$ | Tors 3 $C_3$-$C_7$-$N_8$-$C_9$ | Tors 4 $C_3$-$C_7$-$N_8$-$C_{12}$ | Tors 5 $C_9$-$C_{10}$-$C_{11}$-$C_7$ | Tors 6 $C_2$-$C_3$-$C_7$-$H_1$ | Tors 7 $N_1$-$C_3$-$N_8$-$H_2$ | $d_{N1\text{-}N8}$ | $N^+$ plane height | $N_{ar}$-N**H** distance | Energy (kcal $mol^{-1}$) |
|---|---|---|---|---|---|---|---|---|---|---|---|
| A1(*cis*7) | 91.8 | 192.5 | 81.7 | 315.9 | 357.4 | 329.2 | 252.2 | 4.54 | 1.45 | 5.44 | 24.8 |
| B1(*cis*11) | 273.5 | 192.8 | 82 | 316.2 | 357.7 | 150.8 | 162.3 | 4.54 | −1.46 | 5.58 | 24.8 |
| A2(*cis*8) | 97 | 278.8 | 171 | 49.3 | 359.3 | 338.0 | 350.2 | 4.64 | 1.31 | 4.54 | 26.5 |
| B2(*cis*14) | 279.2 | 278.7 | 170.7 | 48.9 | 358.9 | 160.2 | 254.8 | 4.58 | −1.32 | 4.93 | 26.4 |
| A3(*cis*4) | 112.1 | 216.7 | 110.1 | 341.8 | 33.8 | 350.7 | 295.7 | 4.74 | 1.27 | 5.39 | 25.0 |
| B3(*cis*10) | 294.1 | 216.9 | 110.3 | 341.8 | 34 | 172.5 | 202.9 | 4.47 | −1.27 | 5.46 | 24.8 |
| A4(*cis*13) | 47.1 | 281.9 | 171.2 | 49.2 | 9.2 | 286.3 | 320.0 | 4.31 | 1.20 | 4.19 | 25.9 |
| B4(*cis*6) | 229.5 | 281.9 | 171.4 | 49.3 | 10.8 | 108.7 | 237.7 | 4.81 | −1.24 | 5.20 | 26.2 |
| A5(*cis*12) | 65.3 | 262.7 | 155.2 | 31.5 | 43 | 304.1 | 319.5 | 4.40 | 1.35 | 4.41 | 25.1 |
| B5(*cis*5) | 247.9 | 262.5 | 155.2 | 31.5 | 43.1 | 126.6 | 232.0 | 4.74 | −1.36 | 5.27 | 25.3 |
| A6(*cis*2) | 140.6 | 195.7 | 89.9 | 318.1 | 328.7 | 16.7 | 288.2 | 4.92 | 0.90 | 5.69 | 27.3 |
| B6(*cis*9) | 322.2 | 195.4 | 89.6 | 317.5 | 328.2 | 198.2 | 191.8 | 4.44 | −0.89 | 5.47 | 27.0 |
| A7(*cis*3) | 92.5 | 245.8 | 136.5 | 12.6 | 324.1 | 331.1 | 318.8 | 4.60 | 1.38 | 4.89 | 25.8 |
| B7(*cis*1) | 275 | 246.4 | 137.1 | 13.1 | 324.6 | 153.6 | 226.4 | 4.58 | −1.39 | 5.33 | 25.7 |
| Approximate transition conformation for pyridine-pyrrolidine ring rotations suggested by aiMD | | | | | | | | | | | |
| C1($N_8$–$C_4$) | 194.8 | 277.9 | 170.1 | 44.0 | 32.0 | 91.8 | 86.6 | 4.92 | 0.35 | 5.03 | |
| C2($N_8$–$C_2$) | 31.0 | 185.4 | 71.0 | 305.2 | 354.6 | 281.2 | 194.3 | 4.42 | 0.56 | 5.46 | |

*Table 2.* Geometry details of 10 local minima and approximate transition conformations of protonated *trans* nicotine.

| | Tors 1 $C_2$-$C_3$-$C_7$-$N_8$ | Tors 2 $C_{12}$-$N_8$-$C_7$-$C_{11}$ | Tors 3 $C_3$-$C_7$-$N_8$-$C_9$ | Tors 4 $C_3$-$C_7$-$N_8$-$C_{12}$ | Tors 5 $C_9$-$C_{10}$-$C_{11}$-$C_7$ | Tors 6 $C_2$-$C_3$-$C_7$-$H_1$ | Tors 7 $N_1$-$C_3$-$N_8$-$H_2$ | $d_{N1\text{-}N8}$ | $N^+$ plane height | $N_{ar}$-N**H** distance | Energy (kcal mol$^{-1}$) |
|---|---|---|---|---|---|---|---|---|---|---|---|
| A1(*trans*3) | 113.3 | 161.9 | 160.3 | 287 | 35.9 | 351.0 | 101.3 | 4.72 | 1.26 | 4.77 | 24.1 |
| B1(*trans*1) | 295.8 | 161.8 | 160 | 286.6 | 35.9 | 173.4 | 8.6 | 4.44 | −1.26 | 3.97 | 24.0 |
| A2(*trans*8) | 107.6 | 147.8 | 146.3 | 272.1 | 330.6 | 346.5 | 84.2 | 4.65 | 1.34 | 4.54 | 23.5 |
| B2(*trans*4) | 289.8 | 148 | 146.4 | 272.2 | 330.9 | 168.7 | 354.2 | 4.41 | −1.34 | 3.88 | 23.3 |
| A3(*trans*9) | 86.4 | 81.2 | 82.9 | 204.8 | 357.6 | 324.0 | 13.1 | 4.46 | 1.42 | 4.00 | 25.5 |
| B3(*trans*2) | 268.5 | 81.5 | 83.2 | 205 | 357.9 | 146.1 | 283.7 | 4.55 | −1.42 | 4.43 | 25.5 |
| A4(*trans*7) | 154.7 | 98.4 | 94.9 | 218.4 | 320.4 | 29.9 | 57.3 | 4.94 | 0.65 | 4.80 | 25.9 |
| B4(*trans*11) | 334.8 | 98.4 | 95 | 218.5 | 320.5 | 210.1 | 323.0 | 4.35 | −0.66 | 3.90 | 25.6 |
| A5(*trans*6) | 37.4 | 128.4 | 131.5 | 254.4 | 43.5 | 274.7 | 32.0 | 4.32 | 1.01 | 3.81 | 25.5 |
| B5(*trans*10) | 217.6 | 128.5 | 131.7 | 254.6 | 43.5 | 94.8 | 307.3 | 4.89 | −1.01 | 4.68 | 25.9 |
| Approximate transition conformations for pyridine-pyrrolidine ring rotations suggested by aiMD | | | | | | | | | | | |
| C1($N_8$–$C_4$) | 177.5 | 120.2 | 121.3 | 247.1 | 325.1 | 55.2 | 287.9 | 5.05 | −0.14 | 4.86 | |
| C2($N_8$–$C_2$) | 358.9 | 154.6 | 150.6 | 280.6 | 351.5 | 238.7 | 35.7 | 4.20 | −0.26 | 3.62 | |

plane (B2-*trans*4), or with $N_8$ out-of-plane. (A1-*cis*7) The most stable *cis* conformation was approximately 1.7 kcal mol$^{-1}$ higher in energy than the lowest-energy *trans* conformation.

In addition, examples of two conformations representing approximate transition conformations for rotation of the pyrrolidine ring past the pyridine ring are also included in Tables 1 and 2. These were taken from aiMD simulations and will be discussed in greater detail below. In both the *cis* and *trans* cases, transition conformer C1 corresponds to the cationic center passing close to the pyridine $C_4$ position, while C2 corresponds to the cationic center passing close to the pyridine nitrogen.

Plots of the inter-ring torsion angle (T1) *versus* the pseudo-torsion angle defined by $N_1$-$C_3$-$N_8$-$H_1$ (T7) for these low energy conformations are shown in Figure 3. Illustrating the relative position of two of the most important pharmacophoric points in nicotine, the hydrogen bond-acceptor (pyridyl $N_{ar}$) relative to the N-H of the cationic center. Note the wide range (approximately 90°) for the inter-ring angle (T1) of these local minima, demonstrating substantial adaptability regarding the cationic center's location and orientation. Furthermore, Figure 3a and b for *cis* and *trans* protonated nicotine show projection of the cationic center N–H into four distinct regions of space for these sets of conformations. These differences would lead to very different interactions with the nAChR receptors based on the relative orientation of the cationic center and the hydrogen bond acceptor.

For 3D QSAR, low energy conformers from MM studies are often used as starting points for further geometry optimization and subsequent pharmacophore analysis. To assess the quality of the MM potential energy surface, single point DFT energy calculations were performed at these 24 local minima. Both orbital-based DFT calculations with PW91 or B3LYP functionals, as well as plane-wave based DFT calculations with PBE functional, were used to characterize these conformations. Comparative results are shown in Figure 4a (*cis* nicotine) and b (*trans* nicotine).

All DFT calculations, including the implementation used for aiMD dynamics, provided similar energies for the different conformers of protonated *cis* nicotine (**1a**) and *trans* nicotine (**1b**), with standard deviations across the methods of $\leq$ 0.32 kcal mol$^{-1}$ and 0.40 kcal mol$^{-1}$, respec-

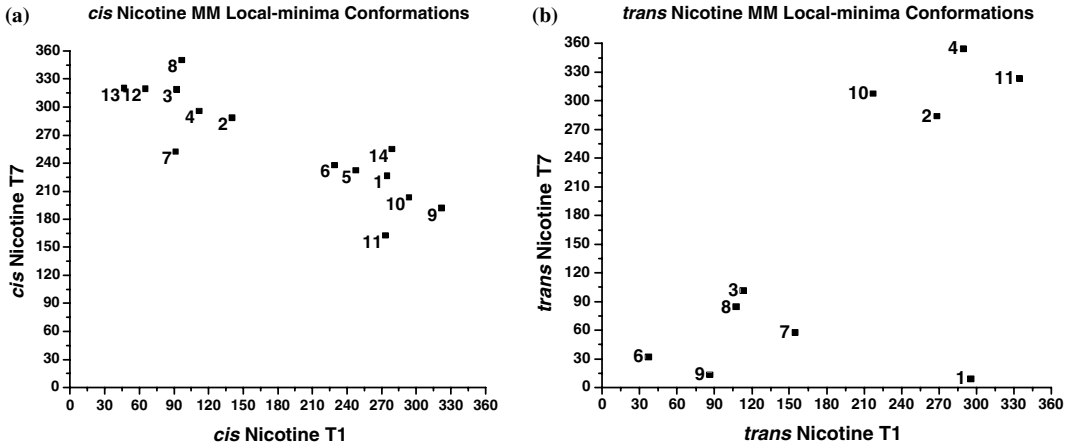


*Figure 3*. Plots for *cis* and *trans* protonated nicotine of inter-ring torsion angle (T1) *vs.* pseudo torsion angle of N–H position (T7), demonstrating the difference in the relative positions of the N–H moiety in the cationic center for these diastereomers. Numbers in Figures 3 and 4 refer to low-energy conformations noted in Table 1 (*cis*) and Table 2 (*trans*), respectively.

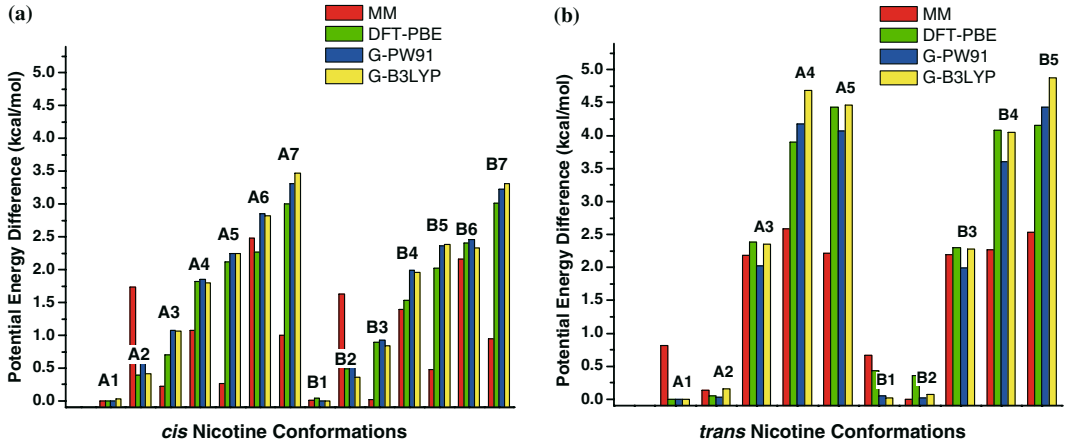


*Figure 4*. Comparative relative potential energy results for DFT and Gaussian shown for *cis* nicotine (a) and *trans* nicotine (b).

tively. The relative order, however, was different from that identified by the molecular mechanics calculations. While all methods identified *cis* A1 (B1), A3 (B3) and *trans* A1 (B1), A2 (B2) as low-energy conformations, MM energies for *cis* A2 (B2) (cationic nitrogen out-of-plane) could have excluded these conformers as starting points for further optimization. Further study of *cis* A2 (B2) would be useful for developing force fields suitable for such systems. For *cis* nicotine, all low-energy conformations have the cationic center out-of-plane, while for trans, either the 3- or 5-position of the pyrrolidine ring is out-of-plane [48].

Interestingly, the quantum calculations predict that *cis* conformer energies increase gradually by around 0.5 kcal $mol^{-1}$ from A1 (B1) to A7 (B7). On the other hand, among *trans* conformers, A1 (B1) and A2 (B2) are significantly more stable than others. They have energies more than 2 kcal $mol^{-1}$ lower than A3 (B3) and more than 4 kcal $mol^{-1}$ lower than A4 (B4) and A5 (B5). This suggests that *cis* conformers have a relative flat potential energy surface while there exist several deep wells in the potential energy surface of the *trans* conformers, behavior not well appreciated by the Tripos force field.

### *Dynamical simulations with aiMD*

For initial aiMD studies, one conformation for both *cis* and *trans* protonated nicotine was randomly selected for canonical MD simulations for

15 ps and 11.4 ps, respectively, at both 800 and 300 K. While the results at 300 and 800 K were qualitatively similar (results not shown), the 800 K trajectories explored substantially more conformational space over the same period. Potential and kinetic energies of typical 800 K simulations varied by 13 kcal $mol^{-1}$ and 0.25 kcal $mol^{-1}$, respectively.

For both **1a** and **1b**, more conformations of the pyrrolidine ring are explored at elevated temperature than at room temperature during the same period of time. Figures 5a and b are plots of observed torsional angles T1 *versus* T7 for *cis* (**1a**) and *trans* (**1b**) nicotine, respectively, while Figures 6a and b are plots of the variation of inter-ring torsion angle (T1) over the course of these same 800 K trajectories.

While *trans* nicotine undergoes 5 inter-ring torsion angle crossings (Figure 6b shows two with the cationic center passing the 4-position of the pyridine ring (C1) – a 180° crossing, and three passing the 2-position (C2) – a 360° crossing) over the course of the 11.4 ps trajectory, *cis* nicotine (**1a;** Figure 6a) had only limited movement around the inter-ring angle, and no rotation to the opposite side of the pyridine ring over the course of the 15 ps trajectory. This indicates a large torsional energy barrier for rotation of the pyrrolidine ring eclipsing the pyridine ring, particularly in the case of *cis* nicotine (**1a**). Even at 800 K, sampling with a simulation of 10–15 ps is not enough to fully explore important regions in the potential energy surface, i.e. those around the known local minima.

Further increase in temperature would likely increase the risk of bond breaking. Two additional ways to increase sampling efficiency were considered: increase the sampling period of a single trajectory; or initiate multiple dynamics runs from different unrelated starting conformations. Given the large rotational barrier for *cis* nicotine, the latter "super-ensemble" approach appeared to be more efficient and was therefore adopted.

All 14 *cis* (**1a**) and 10 *trans* (**1b**) nicotine conformations derived from the MM calculations were selected as starting points. Each were equilibrated at 800 K for 0.5 ps, and then sampled for 14.5 ps (**1a**), or 10.9 ps (**1b**). It is of note that rotation of the inter-ring torsion bond shows considerable hindrance in both cases. While movement towards full rotation occurs frequently, these partial rotations are often non-productive with the cationic center lapsing back to the same side of the pyridine ring, particularly for the cis nicotine diastereomer. In contrast, regardless of the initial conformation, the pyrrolidine ring thoroughly explores conformational space over the course of the simulation.

Based on these observations, data from all ensemble runs for *cis* nicotine (**1a**) was combined to obtain a more complete exploration of conformational space. An ensemble of conformations was also assembled for *trans* nicotine (**1b**); Figure 7. Both **1a** and **1b** show areas with high density of conformations similar to those found as low-energy minima by MM, but with greater conformational range. Very different areas of space are

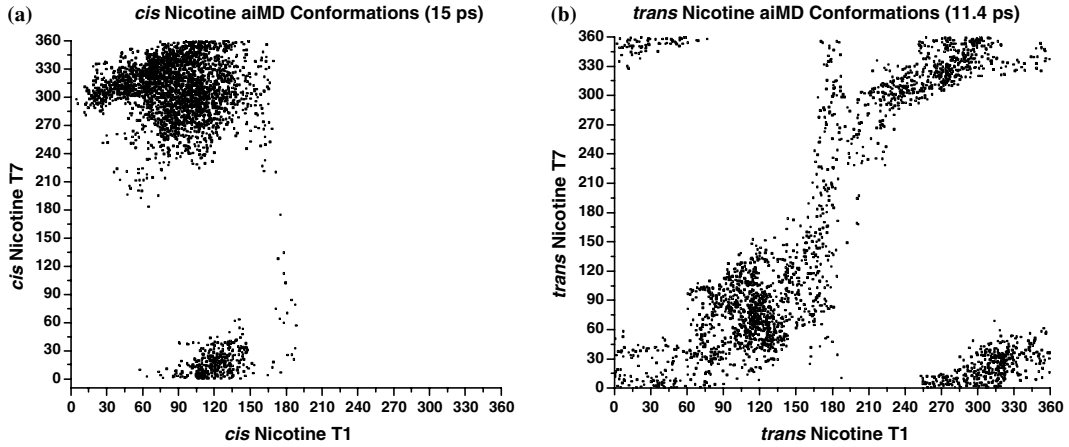


*Figure 5.* Plots of inter-ring torsion angle (T1) vs. T7 for *cis* (**1a**) and *trans* (**1b**) protonated nicotine conformations generated by aiMD over 15 and 11.4 ps, respectively, at 800 K.

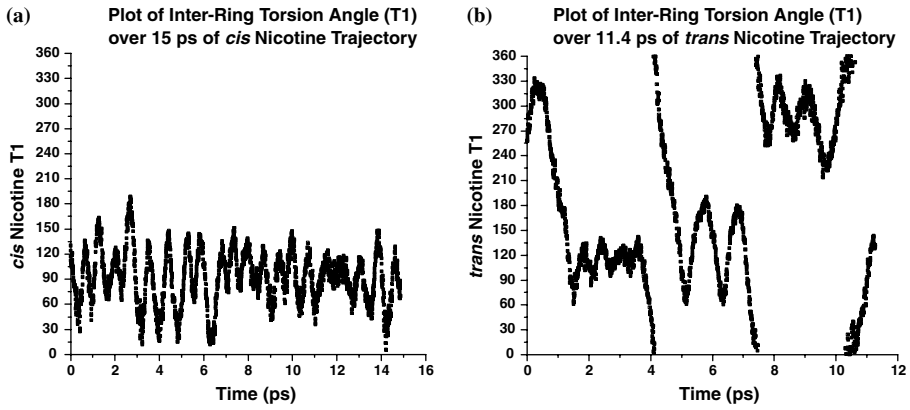


*Figure 6*. Plots of inter-ring torsion angle (T1) *vs*. aiMD trajectory time for *cis* (**1a**) and *trans* (**1b**) protonated nicotine conformations over 15 ps and 11.4 ps simulations, respectively.

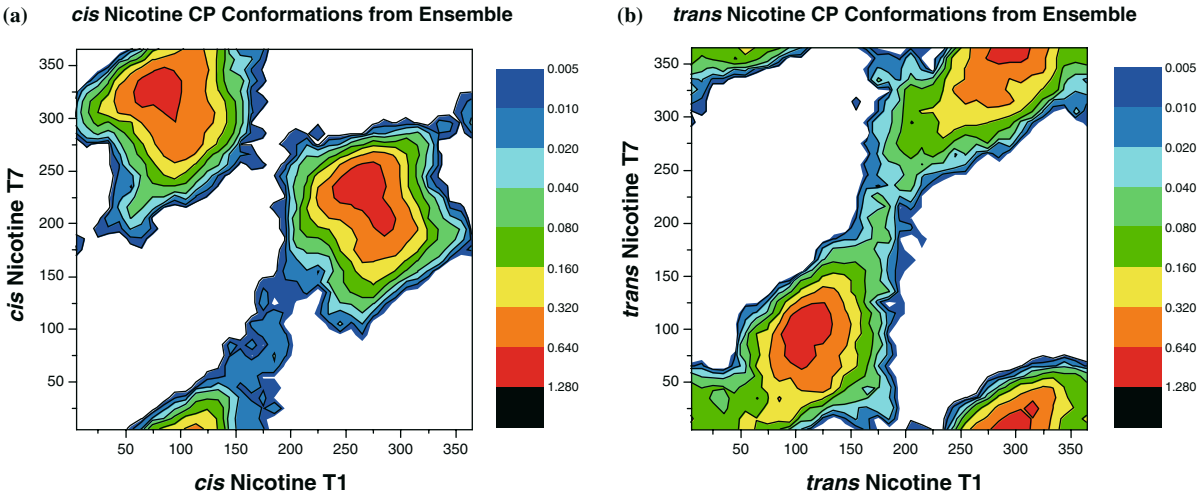


*Figure 7*. Contour plots of percentage (37-by-37 grid) occupancy for inter-ring torsion angle (T1) *vs*. pseudo torsion angle of N–H position for *cis* (**1a**) and *trans* (**1b**) protonated nicotine. Generated by aiMD and summed over all ensemble conformations.

visited by *cis* and *trans* nicotine, with respect to the geometric relationship between the pyridine aromatic nitrogen and cationic center. It is clear that a larger energy barrier is present in the conformational change of *cis* nicotine than is found for *trans* nicotine. Further, the spread of conformational space sampled is larger in *cis* nicotine, suggesting a more flexible pyrrolidine ring.

Since for $\pi$-cation interactions between a ligand and receptor aromatic amino acid residues, it is likely that both the orientation and relative geometry of these features are of importance, we have also examined the distance between the hydrogen bond acceptor and the N–H of the cationic center. A polar plot of the distance between the pyridine nitrogen (N1) and the cationic N–**H** *vs*. the inter-ring torsion angle T1 shown in Figure 8, clearly demonstrates the marked differences between this feature in *cis* (**1a**) and *trans* (**1b**) nicotine. Note that the mean Nar-to-N–**H** distance was found to be 5.07 ($\pm$0.48) Å for **1a** compared to 4.31 ($\pm$0.51) Å for **1b**, and the relative position of the cationic center is shifted considerably between the two diastereomers.

As was seen in the initial trajectory at 800 K for *cis* nicotine, the composite ensembles show rotations around the inter-ring angle to occur much more frequently for *trans* nicotine (**1b**) compared to **1a**. During the 114 ps MD simulation of the *trans* diastereomer ensemble, crossings of the

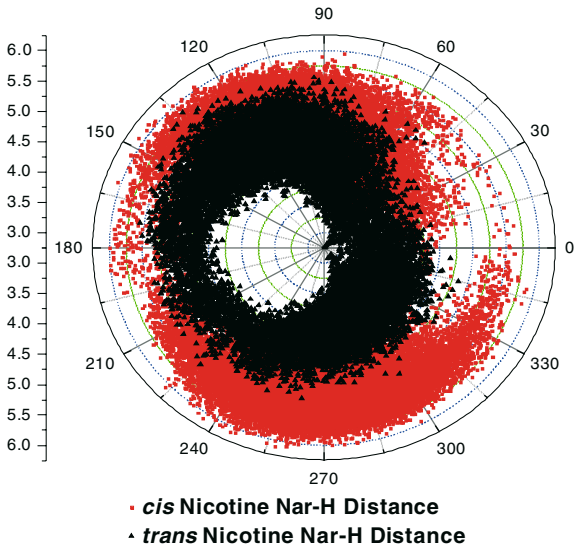


*Figure 8*. Polar plot of inter-ring torsion angle T1 and Nar ($N_1$) to cationic center hydrogen ($H_2$) for *cis* and *trans* protonated nicotine from aiMD. Note significant differences in distance (Y-axis) and distribution.

cationic center passing either the 2- or 4-position of the pyridine ring occurred with similar frequencies, 12 at 180° and 10 at 360°. No single pyrrolidine ring conformation was required during these aiMD simulations to allow inter-ring transitions of the cationic center from one side of the pyridine ring to the other.

In contrast, during 210 ps of aiMD simulation of the *cis* diastereomer, only one 180° transition and three 360° rotations were found for the entire ensemble [49]. Examining the limited number of inter-ring crossings for these aiMD trajectories for *cis* nicotine, shows that a single conformation of the pyrrolidine ring was required to allow transitions of the cationic center from one side of the pyridine ring to the other. For 180° or 360° transitions, only a pyrrolidine conformation where the C7 atom is out-of-plane, and pyridine and methyl groups are equatorial and axial, respectively, allows rotation.

These results are consistent with energy barriers for inter-ring conversions by DFT (Jaguar) geometry scans. Inter-ring crossing energy barriers were 4.6 (T1 = 186–189°) and 3.6 (T1 = 5–10°) kcal $mol^{-1}$, respectively, for *trans* nicotine. Energy barriers are independent of the starting conformation in that two different conformations of the pyrrolidine ring give the same energy barrier, in agreement with the aiMD findings. In contrast, barriers for *cis* nicotine were dependent on the starting conformation of the pyrrolidine ring, and were substantially higher.

A simulation beginning with the pyrrolidine ring with C7 out-of-plane and the pyridine and methyl groups equatorial and axial, respectively, gave inter-ring crossing energy barriers of 7.9 (T1 = 167°) and 6.9 (T1 = 359°) kcal $mol^{-1}$. Starting with a pyrrolidine ring conformation where C7 was again out-of-plane, but the pyridine and methyl groups were axial and equatorial, respectively, or where the C10 atom was out-of-plane with pyridine and methyl groups both equatorial, gave energy barriers of 9.5 (T1 = 201°; 213°) and 8.9 (T1 = 19°; 34°) kcal $mol^{-1}$. In all three cases, these barriers were substantially higher than those for the *trans* case, and explain why for *cis* nicotine, rotation of the pyridine and pyrrolidine rings occurs with much lower frequency. The starting conformation for the lower energy path for *cis* nicotine corresponds to the conformation that appears by aiMD runs to allow rotation around the inter-ring angle. The orientation of the pyridine ring with respect to the methyl group affects the rotation of the pyridine ring, as does the conformation of the pyrrolidine ring. During dynamics, rotation does not occur from other beginning conformations without rearrangement.

### *Dynamical simulations with molecular mechanics*

For comparison, long simulations at 800 K were carried out using two different MM force fields, Tripos and AMBER. Dynamics runs over 200 ps using the Tripos force field at 800 K display a very flexible system with all possible conformations of the pyrrolidine ring represented and multiple rotations around the inter-ring torsion angle for *trans* nicotine, i.e., 5–7 rotations every 15 ps *via* each transition conformation (180° and 360°). *cis* Nicotine showed more hindered rotation, averaging only about 1 transition by either 180° or 360° routes during 15 ps. For both diastereomers, the frequency of inter-ring bond rotation was much higher than that found by aiMD. In contrast, AMBER simulations over 2000 ps (2 ns) of microscopic dynamics for protonated *trans* nicotine gave similar inter-ring transitions compared to

*Table 3*. Relative frequency of rotations around the inter-ring torsion angle per 100 ps of MD, for AMBER and aiMD.

| | AMBER | | aiMD | |
|---|---|---|---|---|
| Approximate tors 1 | *Cis* nicotine | *Trans* nicotine | *Cis* nicotine | *Trans* nicotine |
| 0° | 0.15 | 5 | 1.4 | 8.8 |
| 360° | 0.08 | 4.2 | 0.5 | 10.5 |

aiMD, with approximately 1 rotation occurring by both the 180° and 360° pathway during 15 ps of MD. AMBER simulations of *cis* nicotine, however, showed much more constrained inter-ring rotation, averaging only 1–2 rotations by either 180° or 360° transitions over the entire 2 ns trajectory time period. Table 3 shows the relative frequency of inter-ring crossings per 100 ps of either AMBER or aiMD.

Showing the distribution of conformations by inter-ring angle, Figure 9 illustrates differences in relative populations of conformations generated during aiMD and AMBER dynamics. To further identify specific conformations where inter-ring torsion angle was insufficient to discriminate, a separate analysis for two 14.5 ps aiMD *cis* nicotine trajectories was carried out to more closely examine relative populations. Each aiMD conformation was compared by RMSD of the heavy atoms to each original low-energy MM-derived conformation. This analysis found similar populations to those shown for both the A and B conformations in Figure 9, and allowed for identification of the overlapping conformations.

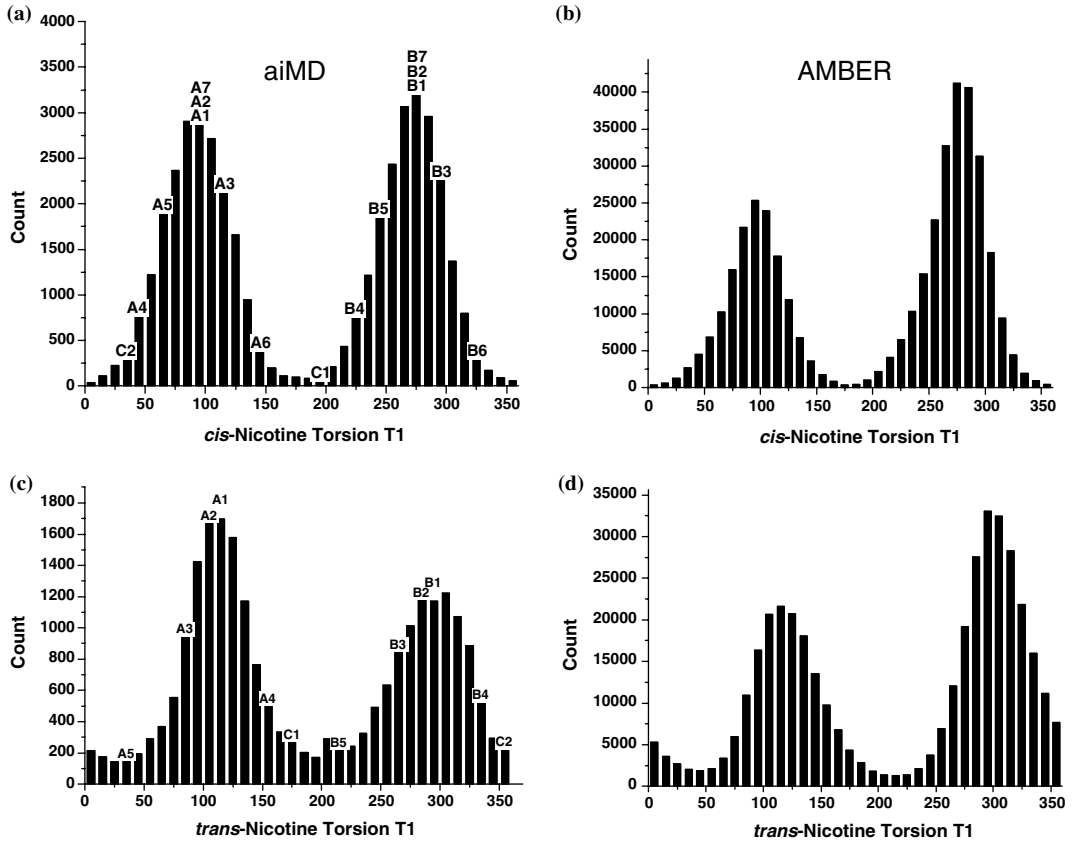


*Figure 9*. Distribution of inter-ring torsion angle (T1) for *cis* (**a, b**) and *trans* (**c, d**) protonated nicotine from aiMD and Amber MM trajectories. Note that the two methods show a difference in populations of cationic group locations relative to the pyridine ring orientation.

For conformers A1, A2 and A7 (T1 between 90 and 100°), the relative ratio of occurrence was 1:1.8:1.9 (for B1, B2 and B7, the ratio was 1:1.6:1.9). This distribution likely arises from a preference for the pseudo-equatorial pyridine, pseudo-axial methyl orientation for A2 (B2) and A7 (B7), *versus* the pseudo-axial pyridine, pseudo-equatorial methyl orientation found in A1 (B1). As would be expected on the basis of the single point energy calculations, A6 was sampled very infrequently, in line with the composite results in Figure 9. However, both A1 and A4 are less frequently sampled than A2 (B2), A3 (B3), A5 (B5) and A7 (B7), with A7 (B7), the highest energy conformation from the single-point calculations, showing the highest ensemble (and individual) populations of any conformation [50]. Thus, the single point calculations do not accurately reflect the relative distributions of these conformations revealed by molecular dynamics. The single point calculations give the potential energy surface and the curvature of the energy surface around that single point, while the relative distributions from molecular dynamics provide a general picture of the free energy surface, with the explicit inclusion of entropy. Using single-point calculations of individual low-energy conformers to represent the complex energy surface can provide misleading results if the assumption is made that the relative energy of the lowest energy conformer necessarily reflects ensemble populations.

While aiMD trajectories for *cis* nicotine show conformations with the cationic center on either the A- or the B-side of the pyridine ring sampled at an approximately equal extent. This was not the case for the AMBER trajectory where the B conformations were sampled with greater frequency. Note that the AMBER trajectory was repeated two times, starting with both a B and an A conformation, to assure that the results were not biased by the initial conformation. Both trajectories showed the same preference for B conformations.

The aiMD results for *trans* protonated nicotine showed the low-energy conformations from single point calculations, i.e., A1 and A2, sampled to a much larger extent than B1 and B2, with both sets sampled to a greater extent than A3 (B3). As expected, the two highest energy conformers from single-point calculations, A4 (B4) and A5 (B5), were explored infrequently. AMBER simulations predict opposite tendencies, with B-side conformations more frequently sampled compared to the A-side conformations. The geometric relationship of the cationic center and the putative hydrogen-bond acceptor, *i.e.* the pyridyl nitrogen, represented by these A and B orientations have implications for nAChR binding. A cationic center tending to one side of the pyridine ring for the S-isomer of nicotine, would imply the opposite side preference for the R-isomer.

Thus, the 50-fold difference in binding affinity for the two (R and S) nicotine enantiomers [51] may be related to the diastereomerism generated upon protonation. One ensemble of conformations for an enantiomer of either the *cis* or *trans* diastereomers, may show a preference for the binding orientation, while the mirror-image enantiomer would be expected to show a preference for a non-productive orientation. A further factor that has not as yet been investigated but may influence binding is the difference in the entropic component for the *cis versus trans* configurations. In this study, relatively free inter-ring rotation is found for *trans* nicotine while the *cis* nicotine diastereomer is more highly constrained, in agreement with the calculated entropy for protonated *trans* nicotine (gas phase) described by Elmore and Dougherty [6]. However, if one of the favored conformations for *cis* nicotine is close to the actual binding conformation at the receptor, then less reorganization of the overall system would be required and could favor binding in that configuration. We are currently investigating both diastereomers as potential binding conformations.

## Conclusions

Current computational protocols typically utilized to describe small molecules do not fully account for electronic structure and more importantly, do not characterize dynamic behavior. We have carried out classical and quantum studies, examining both single point and dynamical behavior, of two protonation-induced diastereomers of the nAChR agonist S-nicotine, *cis* (S,S)-nicotine and *trans* (R,S)-nicotine. Results of these studies show that protonation-induced isomerism produce significant differences with regards to the relative geometric relationship of the cationic center and the putative hydrogen-bond acceptor. These differ-

ences have implications for interactions with the nAChRs via both conformational preference and electronic effects (through ligand-receptor $\pi$-cation interactions) that are likely to influence the behavior of each disatereomer in its interaction with a target protein.

A series of relatively short trajectories was carried out at 800 K, and then combined to form an ensemble describing the conformational behavior of each diastereomer. This appeared to be a reasonable approach since aiMD studies for both diastereomers, carried out for 10 ps or longer at 800 K, yielded similar results to longer simulations – 40 ps or more at 300 K. This "super ensemble" approach is a common way to investigate systems where a single trajectory for long time at lower temperature is computationally demanding. We are confident that convergence was approached for these studies.

As might be expected, the two diastereomers displayed markedly different dynamical behaviors, not only with respect to geometry, but also with respect to their ability to sample conformational space. For the *trans* diastereomer, rotation around the inter-ring torsional bond was relatively unhindered for both methods. Sampled positions of the cationic center identified by AMBER and aiMD showed an opposite preference. One would not expect a purely symmetrical distribution of the location of the cationic center on both sides of the pyridine ring system. This particular degree of freedom should be affected by the proximity of the formal charge on the 5-membered ring to the conjugated electrons in the aromatic ring.

Examination of the *cis* diastereomer by both methods showed inter-ring crossings to be much more infrequent, with only four completed transitions in a super ensemble corresponding to over 200 ps of simulation time (aiMD) and 9 rotations over 4 ns of AMBER simulation. This difference is likely a consequence of the empirical potential functions and atom-centered charges in the AMBER force field. In general, less frequent rotations for the *cis* diastereomer are in agreement with the higher estimated energy barrier for inter-ring crossing for the *cis vs*. the *trans* diastereomer, and is likely to arise from more severe steric hindrance by the methyl group. Rotation around the inter-ring bond was also found to be dependent on the conformation of the pyrrolidine ring. Since an accurate representation of a compound's conformational behavior may play a critical role in the understanding of how it interacts with a target receptor, such differences may be significant for our understanding of interactions with the nAChRs.

We have also shown that single point calculations based on individual low-energy conformations as starting points for examination of the conformational energy surface may provide a misleading impression of likely binding conformations. Indeed, the free energy surface rather than the potential energy surface should be taken into account. An ensemble approach, based on either MM or aiMD provides a feasible means of exploring the free energy surface. Further, although MM simulations are extremely cost effective computationally, significant time and effort are required to parameterize terms that are not part of a standard MM force field, in addition to a lack of treatment of the dynamical nature of electrons and the related electronic effects.

Currently, we are fully characterizing the ensemble behavior of R- and S-, *cis* and *trans* nicotine, nornicotine, and other nAChR agonists, in attempts to identify relationships with their observed differences in binding affinities at nAChRs. Other areas under investigation include the use of Wannier functions to examine conformational effects on the wavefunction, and examining other methods to aid in analysis of the data generated from such studies, for example, Markov operators via self-organizing maps using neural networks for subsequent Perron cluster analysis [52, 53].

## References


1. Bencherif, M. and Schmitt, J.D., Curr. Drug Target CNS. Neurol. Disord., 1 (2002) 349.
2. Barlow, R.B., Howard, J.A.K. and Johnson, O., Acta Crystallogr., Section C: Cryst. Struct. Commun., C42 (1986) 853.
3. Koo, C.H. and Kim, H.S., Taehan Hwahakhoe Chi, 9 (1965) 134.
4. Chynoweth, K.R., Ternai, B., Simeral, L.S. and Maciel, G.E., Mol. Pharmacol., 9 (1973) 144.
5. Whidby, J.F. and Seeman, J.I., J. Org. Chem., 41 (1976) 1585.
6. Elmore, D.E. and Dougherty, D.A., J Org. Chem., 65 (2000) 742.
7. Gohlke, H., Schwarz, S., Gundisch, D., Tilotta, M.C., Weber, A., Wegge, T., and Seitz, G., J. Med. Chem., 46 (2003) 2031.

8. Teague, S.J., Nat. Rev. Drug Discov., 2 (2003) 527.
9. Mattos, C. and Ringe, D., Multiple Binding Modes, In Kubinyi, H. (Ed.), 3D QSAR in Drug Design: Theory Methods and Applications, Kluwer Academic Publishers, Dordrecht, 1993, pp. 226–254.
10. Zacharias, N. and Dougherty, D.A., Trends Pharmacol. Sci., 23 (2002) 281.
11. Gallivan, J.P.D.D.A., J. Am. Chem. Soc., 122 (2000) 870.
12. Schmitt, J.D., Sharples, C.G. and Caldwell, W.S., J. Med. Chem., 42 (1999) 3066.
13. Dougherty, D.A., Science, 271 (1996) 163.
14. Ma, J.C. and Dougherty, D.A., Chem. Rev., 97 (1997) 1303.
15. Zacharias, N. and Dougherty, D.A., Trends Pharmacol. Sci., 23 (2002) 281.
16. Weiner, P.K. and Kollman, P.A., J. Comput. Chem., 2 (1981) 287.
17. Case, D.A., Pearlman, D.A., Caldwell, J.W., Cheatham III, T.E., Wang, J., Ross, W.S., Simmerling, C.L., Darden, T.A., Merz, K.M., Stanton, R.V.,.Cheng, A.L., Vincent, J.J., Crowley, M., Tsui, V., Gohlke, H., Radmer, R.J., Duan, Y., Pitera, J., Massova, I., Seibel, G.L., Singh, U.C., Weiner, P.K. and Kollman, P.A. Amber[7]. University of California, San Francisco, CA, 2002.
18. Pearlman, D.A., Case, D.A., Caldwell, J.W., Ross, W.S., Cheatham, T.E. III, DeBolt, S., Ferguson, D., Seibel, G. and Kollman, P., Comput. Phys. Commun., 91(1–3) (1995) 1.
19. Car, R., and Parrinell, M., Phys. Rev. Lett., 55 (1985) 2471.
20. Sulpizi, M., Laio, A., VandeVondele, J., Cattaneo, A., Rothlisberger, U., and Carloni, P., Proteins, 52 (2003) 212.
21. Minehardt, T.J., Marzari, N., Cooke, R., Pate, E., Kollman, P.A. and Car, R., Biophys. J., 82 (2002) 660.
22. Carloni, P., Rothlisberger, U. and Parrinello, M., Acc. Chem. Res., 35(6) (2002) 455.
23. Tse, J.S., Annu. Rev. Phys. Chem., 53 (2002) 249.
24. Car, R., Quant. Struct.-Act. Relat., 21(2) (2002) 97.
25. Hohenberg, P. and Kohn, W., Phys. Rev., 136 (1964) B864.
26. Kohn, W. and Sham, L., Phys. Rev., 140 (1965) A1133.
27. Sybyl Molecular Modeling Software [Version 6.9] 2003. Tripos, Inc., St. Louis, MO, USA.
28. Li, Z. and Scheraga, H.A., Proc. Natl. Acad. Sci. USA, 84 (1987) 6611.
29. Chang, G., Guida, W.C. and Still, W.C., J. Am. Chem. Soc., 111 (1989) 4379.
30. Saunders, M., J. Am. Chem. Soc., 109 (1987) 3150.
31. Saunders, M., Houk, K.N., Wu, Y.D., Still, W.C., Lipton, M., Chang, G. and Guida, W.C., J. Am. Chem. Soc., 112 (1990) 1419.
32. Case, D.A., Pearlman, D.A., Caldwell, J.W., Cheatham III, T.E., Wang, J., Ross, W.S., Simmerling, C.L., Darden, T.A., Merz, K.M., Stanton, R.V., Cheng, A.L., Vincent, J.J., Crowley, M., Tsui, V., Gohlke, H., Radmer, R.J., Duan, Y., Pitera, J., Massova, I., Seibel, G.L., Singh, U.C., Weiner, P.K. and Kollman, P.A., Amber[7]. University of California, San Francisco, CA, 2002.
33. Cornell, W.D., Cieplak, P., Bayly, C.I., Gould, I.R., Merz, K.M., Jr., Ferguson, D.M., Spellmeyer, D.C., Fox, T., Caldwell, J.W. and Kollman, P.A., J. Am. Chem. Soc., 117 (1995) 5179.
34. Bayly, C.I., Cieplak, P., Cornell, W. and Kollman, P.A., J. Phys. Chem., 97 (1993) 10269.
35. Frisch, M.J., Trucks, G.W., Schlegel, H.B., Scuseria, G.E., Robb, M.A., Cheeseman, J.R., Zakrzewski, V.G., Montgomery, J.A., Stratmann, R.E., Burant, J.C., Dapprich, S., Millam, J.M., Daniels, A.D., Kudin, K.N., Strain, M.C., Farkas, O., Tomasi, J., Barone, V., Cossi, M., Cammi, R., Mennucci, B., Pomelli, C., Adamo, C., Clifford, S., Ochterski, J., Petersson, G.A., Ayala, P.Y., Cui, Q., Morokuma, K., Malick, D.K., Rabuck, A.D., Raghavachari, K., Foresman, J.B., Cioslowski, J., Ortiz, J.V., Stefanov, B.B., Liu, G., Liashenko, A., Piskorz, P., Komaromi, I., Gomperts, R., Martin, R.L., Fox, D.J., Keith, T., Al-Laham, M.A., Peng, C.Y., Nanayakkara, A., Gonzalez, C., Challacombe, M., Gill, P.M.W., Johnson, B.G., Chen W., Wong, M.W., Andres, J.L., Head-Gordon, M., Replogle, E.S. and Pople, J.A., Gaussian 98 (Revision A1). Gaussian, Inc, Pittsburgh, PA, 1998.
36. Minehardt, T.J., Cooke, R., Pate, E., and Kollman, P.A., Biophys. J., 80 (2001) 1151.
37. Wang, J., Wang, W. and Kollman, P.A., Antechamber: An Accessory Software Package for Molecular Mechanical Calculations. Abstracts of Papers, 222nd ACS National Meeting, Chicago, IL, USA, August 26–30, 2001, (2001) COMP-135.
38. Berendsen, H.J.C., Postma, J.P.M., Van Gunsteren, W.F., DiNola, A. and Haak, J.R., J. Chem. Phys., 81 (1984) 3684.
39. Becke, A.D., J. Chem. Phys., 98 (1993) 5648.
40. Perdew, J.P., Chevary, J.A., Vosko, S.H., Jackson, K.A., Pederson, M.R., Singh, D.J. and Fiolhais, C., Phys. Rev. B: Condensed Matter, 46 (1992) 6671.
41. Perdew, J. and Yang, W., Phys. Rev. B, 45 (1992) 13244.
42. Laasonen, K., Pasquarello, A., Car, R., Lee, C. and Vanderbilt, D., Phys. Rev. B: Condensed Matter Mater. Phys., 47 (1993) 10142.
43. Giannozzi, P., De Angelis, F. and Car, R., J. Chem. Phys., 120(13) (2004) 5903.
44. Perdew, J.P., Burke, K. and Ernzerhof, M., Phys. Rev. Lett., 77 (1996) 3865.
45. Nose, S., Prog. Theor. Phys. Suppl. 103, (1991) 1.
46. Schrodinger, L.L.C. Jaguar Version 4.1. 2004. Portland, OR, USA.
47. Values for the 7 torsion angles listed in Figure 1, as well as the distance from the pyridine nitrogen to the cationic center nitrogen (N1-N8), N1-NH distance and the height above the plane of the pyridine ring of the cationic center nitrogen are also provided. Note that low-energy conformations were identified that correspond to those examined by Elmore and Dougherty (Ref. 6). A1(*cis*7) corresponds to *cis* + A from that paper, while B1(*cis* 11), A1(*trans* 3) and B1(*trans*1) correspond to *cis* + B, *trans* + A and *trans* + B, repectively.
48. Using Jaguar, full minimization at the DFT level (6-311G**) followed by further refinement (HF, CC-PVTZ(-f)) of all MM *cis* and *trans* nicotine conformations gave similar conformations to those found by MM, but with a somewhat more limited range for the inter-ring torsion angle. An exhaustive search at the DFT level would have likely shown additional conformations.
49. For aiMD trajectories carried out on protonated *cis* nicotine at 300 K (starting with *cis* A3), the conformation with the lowest energy (*cis* A1) was not found during 10 ps of dynamics. This implies a relatively large energy barrier between *cis* A1 and *cis* A3, making MD at elevated

temperature necessary to thoroughly sample conformational space for the pyrrolidine ring.
50. It is of note that in a similar random search on *cis* nicotine, but using the MMFF force field27, A7 and B7 were also identified as the highest energy conformations of those found.
51. Schmitt, J.D., Curr. Med. Chem., 7 (2000) 749.
52. Schutte, Ch. and Cordes, F., On Dynamical Transitions Between Conformational Ensembles. Molecular Dynamics on Parallel Computers, Workshop, Juelich, Feb. 8–10, 1999, pp. 32–45. 2000.
53. Fischer, A., Cordes, F. and Schutte, C., Comput. Phys. Commun., 121–122 (1999) 37.